

Received August 22, 2019, accepted September 1, 2019, date of publication September 4, 2019, date of current version September 18, 2019.

Digital Object Identifier 10.1109/ACCESS.2019.2939418

Impact Angle Constrained Three-Dimensional Integrated Guidance and Control Based on Fractional Integral Terminal Sliding Mode Control

XINGHE ZHOU¹, WEIHONG WANG¹, ZHENGHUA LIU¹, CHEN LIANG¹, AND CHAO LAI²

¹School of Automation Science and Electrical Engineering, Beihang University, Beijing 100191, China

²Navigation and Control Technology Research Institute of China North Industries Group Corporation, Beijing 100089, China

Corresponding author: Xinghe Zhou (DL4008801@163.com)

ABSTRACT In this paper, considering a class of skid-to-turn (STT) missile with impact angle constraint to intercept the maneuvering target, a three-dimensional integrated guidance and control law based on the fractional integral terminal sliding mode control (FITSMC) scheme is proposed. Firstly, a three-dimensional integrated guidance and control model is established for missile-target relative motion and nonlinear missile dynamics with multiple system uncertainties and unknown disturbances. Secondly, in order to achieve the desired impact angle in finite-time without singularity, a novel nonsingular FITSMC scheme is employed to construct the sliding surface, and a modified filter is applied to dynamic surface control design. Also, an extended state observer is introduced to estimate and compensate the system uncertainties and unknown disturbances. Then, a robust integrated guidance and control scheme with impact angle constraint is developed using aforementioned techniques. Furthermore, the finite-time stability of the closed-loop system is proven based on Lyapunov theory. Finally, the effectiveness and robustness of the proposed integrated guidance and control algorithm are verified through numerical simulations.

INDEX TERMS Integrated guidance and control, impact angle constraint, fractional integral terminal sliding mode control, finite-time convergence, dynamic surface control.

I. INTRODUCTION

Due to the increasingly extensive application in modern warfare, missiles have received more and more attention. The classical design approach of missile guidance and control system treats the guidance loop and the control loop separately. However, this design method may restrict the performance of missile system. To overcome this problem, a new design idea called integrated guidance and control (IGC) is proposed for the first time [1]. The IGC method is helpful to overcome the problem of excessive design iterations and high costs caused by designing each subsystem separately. As of now, various control methods have been introduced to design the IGC law, for instance small-gain method [2], [3], linear quadratic regulator [4], [5], back-stepping control [6], [7], and so on. It is noted that the systems for STT missiles including uncertainties, external disturbances, and physical limitations of actuators. So the IGC law needs to be robust and effective enough against the disturbances and uncertainties.

The associate editor coordinating the review of this manuscript and approving it for publication was Jianyong Yao.

Sliding mode control (SMC) has been proved to against system uncertainties and external disturbances with strong robustness [8], [9]. Owing to the above advantages, SMC method has been widely used in IGC design [10], [11]. A sliding mode controller [12] is proposed for STT missiles to overcome the coupling effect. Based on sliding mode control approach, an adaptive nonlinear control law directly gives the fin deflection command [13]. Also in [14], a three-dimensional (3-D) IGC system based on novel adaptive sliding mode control method is proposed for Unmanned Combat Aerial Vehicles in the process of autonomous attack occupation. However, those SMC methods can only guarantee the asymptotic convergence of IGC system.

In recent years, terminal sliding mode control (TSMC) has been demonstrated to achieve finite time convergence and to against uncertainties with better robustness [15], [16]. TSMC method has been successfully applied in IGC design [17], [18]. However, TSMC has a singularity problem that may lead to negative results. To overcome the singularity problem, the nonsingular TSMC method is presented in the

works [19]–[21]. An adaptive sliding mode fault-tolerant guidance law [19] is developed using passive fault-tolerant control method and a nonsingular fast terminal sliding mode control manifold. In [20], based on the nonsingular terminal sliding mode, an impact angle constrained guidance law is designed to intercept the virtual target in finite time. The nonsingular TSMC and dynamic surface control [21] are incorporated to design the IGC law. As a new form of nonsingular TSMC, integral TSMC (ITSMC) is proposed in recent years. For robust output tracking of relative-degree-one systems with uncertainty and disturbance, ITSMC is derived using sign and fractional integral terminal sliding modes [22], the singularity problem in traditional TSMC is avoided. In [23], an adaptive nonsingular ITSMC scheme is proposed, the better robustness is acquired for trajectory tracking of autonomous underwater vehicles with dynamic uncertainties and external disturbances. The application on missile control verifies the effectiveness of the ITSMC. A fast nonsingular ITSMC is proposed for interceptors [24], which guarantees the fast convergence of line-of-sight (LOS) angular rates and the system robustness for uncertainties. In our work, a novel IGC law based on nonsingular FITSMC scheme is proposed for missiles. The nonsingular FITSMC scheme guarantees the finite-time convergence of the tracking errors.

Due to the strict feedback form of IGC model, back-stepping technique is an effective approach to design IGC scheme [6]. However, the back-stepping technique suffers from the problem of “explosion of terms” caused by the repeated differentiations of the virtual control signals. To overcome this drawback, the dynamic surface control (DSC) was adopted to design IGC law in [25]. However, finite-time convergence is not considered in traditional DSC method. In this paper, a modified filter is applied to the DSC design, and the novel DSC method not only addresses the problem of “explosion of terms” but also achieves finite-time convergence.

In the IGC system, various uncertainties and disturbance always bring adverse effects on the performance and robustness of the system. There exists a lot of disturbance estimating methods, such as disturbance observer [26], extended state observer (ESO) [27], neural network [28], etc. ESO can less depend on model information to estimate uncertainty and disturbance. In this work, ESO [27] is applied to estimate the uncertainties and disturbances existing in each loop of back-stepping design.

To improve the lethality of missile’s warhead when intercepting targets [29], impact angle constraint needs to be considered, such as anti-ship missile, anti-tank missile, and anti-ballistic missile. A new guidance law is proposed [30], which is applicable for head-pursuit engagement with negative time-varying navigation ratio. Some attempts have been made on the design of IGC law with impact angle constraint [31]. To achieve the desired terminal impact angle, a new IGC law is proposed for a homing missile [32]. In order to intercept the ground fixed target and ground maneuvering target, a new IGC law is investigated for a STT homing

missile with impact angle constraints [33]. Also in [34], a new robust 3-D IGC method cater to impact angle constraints is designed for STT hypersonic missile with high uncertainties. In this paper, the line-of-sight angles are defined as the impact angles, and the proposed IGC law ensures the missile capture the target with desired impact angles.

The main contributions of this paper are summarized as follows: 1) A novel nonsingular FITSMC scheme is proposed, which guarantees the finite-time convergence of the tracking errors and overcomes the singularity problem in conventional TSMC. 2) A modified filter is applied to DSC method design. Compared with traditional DSC method, the novel DSC method not only addresses the problem of “explosion of terms”, but also achieves finite-time convergence. 3) A novel IGC law is formulated with nonsingular FITSMC scheme to achieve the missile with desired impact angles intercepting maneuvering target.

This paper is organized as follows. In Section II, the mathematical model for the 3-D engagement dynamics and missile dynamics is established. Then, the nonsingular FITSMC scheme is used to design the 3-D IGC law in Section III. Numerical simulations are performed to validate the effectiveness of the proposed approach in Section IV. Finally, conclusion is made in Section V.

II. MODEL DESCRIPTION

In this section, the interception geometry between missile and target is analyzed. Then, the IGC model is established.

A. PRELIMINARIES AND BACKGROUNDS

Before studying IGC model, coordinate systems are defined as follows:

Definition 1: $A\text{-}xyz$ denotes the inertial coordinate system. The origin A of the inertial coordinate system is located at the missile’s launch point; the $A\text{-}x$ axis coincides with the intersecting line of the ballistic plane and the horizontal plane; the $A\text{-}y$ axis points upwards along the local gravity vector; the $A\text{-}z$ axis direction completes the right-handed coordinate system.

Definition 2: $O\text{-}x_4y_4z_4$ denotes the line-of-sight coordinate system. The origin O of the LOS coordinate system is located at the missile’s center of mass; the $O\text{-}x_4$ axis coincides with the line of sight, with the $O\text{-}x_4$ axis pointing towards the target; the $O\text{-}y_4$ axis is located within the vertical plane containing the LOS, and perpendicular to the $O\text{-}x_4$ axis; the $O\text{-}z_4$ axis direction completes the right-handed coordinate system.

As shown in Fig.1 $O\text{-}x_1y_1z_1$ denotes the missile body coordinate system, $O\text{-}x_3y_3z_3$ denotes the velocity coordinate system; α and β respectively denote attack angle and sideslip angle.

B. INTEGRATED GUIDANCE AND CONTROL MODEL

The interception geometry between missile and target in three-dimensional space is depicted in Fig. 2 where $O\text{-}x_2y_2z_2$ denotes the ballistic coordinate system, M and T denote the missile and target, respectively.

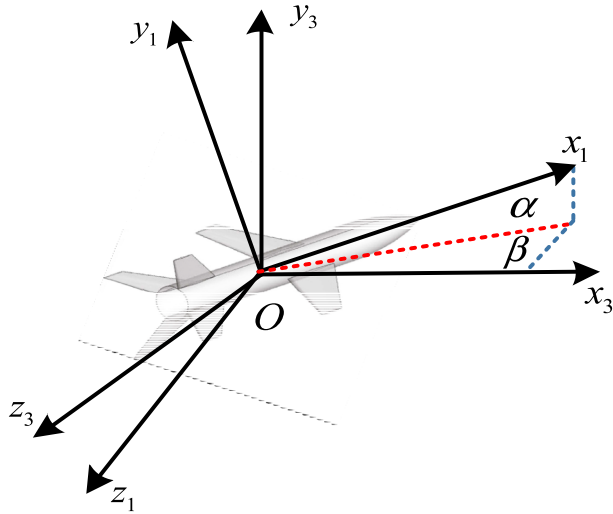


FIGURE 1. The relationship between the missile body coordinate system and the velocity coordinate system.

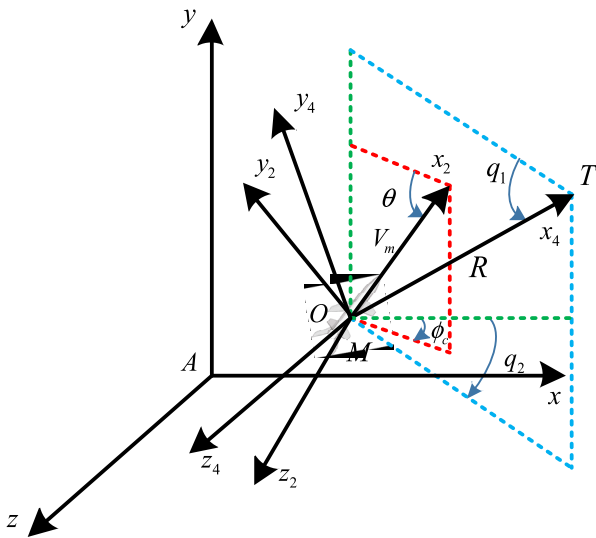


FIGURE 2. Missile-target interception geometry in three-dimensional space.

The missile-target relative motion in LOS coordinate system can be described as follows [35]

$$\begin{cases} \dot{R} = V_{tx4} - V_m \cos \theta \cos q_1 \cos(q_2 - \phi_c) - V_m \sin \theta \sin q_1 \\ R\dot{q}_1 = V_{ty4} - V_m \sin \theta \cos q_1 + V_m \cos \theta \sin q_1 \cos(q_2 - \phi_c) \\ -R\dot{q}_2 \cos q_1 = V_{tz4} - V_m \cos \theta \sin(q_2 - \phi_c) \end{cases} \quad (1)$$

where R denotes missile-target relative distance; q_1 and q_2 denote elevation angle and azimuth angle of LOS; V_m , θ , and ϕ_c respectively denote the speed, flight path angle, and heading angle of missile; $V_{t4} = [V_{tx4}, V_{ty4}, V_{tz4}]^T$ denotes the target velocity in the LOS coordinate system.

In this paper, the trust force of missile is assumed almost zero during the terminal phase, and the velocity of missile is assumed to be nearly invariable in terminal guidance.

The dynamics equations of missile can be expressed as [31]

$$\begin{cases} mV_m\dot{\theta} = Y \cos \gamma_v - Z \sin \gamma_v - mg \cos \theta \\ -mV_m\dot{\phi}_c \cos \theta = Y \sin \gamma_v + Z \cos \gamma_v \end{cases} \quad (2)$$

where Y and Z respectively denote lift force and side force; γ_v denotes velocity deflection angle; m and g respectively denote mass of missile and acceleration of gravity.

Combining (1) and (2), the differential equations with respect to angular speed of LOS can be acquired.

$$\begin{cases} \ddot{q}_1 = -\dot{q}_2^2 \sin q_1 \cos q_1 - \frac{f_q}{mR} (Y \cos \gamma_v - Z \sin \gamma_v - mg \cos \theta) \\ \quad - \frac{\sin q_1 \sin(q_2 - \phi_c) (Y \sin \gamma_v + Z \cos \gamma_v)}{mR} \\ \quad - \frac{2\dot{R}\dot{q}_1}{R} + \frac{a_{ty4}}{R} + dq_1 \\ \ddot{q}_2 = 2\dot{q}_1\dot{q}_2 \tan q_1 + \frac{\cos(q_2 - \phi_c)}{mR \cos q_1} (Y \sin \gamma_v + Z \cos \gamma_v) \\ \quad - \frac{\sin \theta \sin(q_2 - \phi_c)}{mR \cos q_1} (Y \cos \gamma_v - Z \sin \gamma_v - mg \cos \theta) \\ \quad - \frac{2\dot{R}\dot{q}_2}{R} - \frac{a_{tz4}}{R \cos q_1} + dq_2 \end{cases} \quad (3)$$

where $f_q = \cos \theta \cos q_1 + \sin \theta \sin q_1 \cos(q_2 - \phi_c)$; dq_1 and dq_2 denote the system uncertainties; a_{ty4} and a_{tz4} denote the acceleration vectors of the target in the LOS coordinate system.

The attitude dynamic equations of missile are shown as follow [25]

$$\begin{cases} \dot{\alpha} = -\omega_x \cos \alpha \tan \beta + \omega_y \sin \alpha \tan \beta + \omega_z \\ \quad - \frac{Y}{mV_m \cos \beta} + \frac{g}{V_m \cos \beta} \cos \theta \cos \gamma_v \\ \dot{\beta} = \omega_x \sin \alpha + \omega_y \cos \alpha + \frac{Z}{mV_m} + \frac{g}{V_m} \cos \theta \sin \gamma_v \\ \dot{\gamma}_v = \omega_x \cos \alpha \sec \beta - \omega_y \sin \alpha \sec \beta - \frac{g}{V_m} \cos \theta \cos \gamma_v \tan \beta \\ \quad + \frac{Y(\tan \theta \sin \gamma_v + \tan \beta) + Z \tan \theta \cos \gamma_v}{mV_m} \end{cases} \quad (4)$$

$$\begin{cases} \dot{\omega}_x = \frac{J_y - J_z}{J_x} \omega_y \omega_z + \frac{M_x}{J_x} \\ \dot{\omega}_y = \frac{J_z - J_x}{J_y} \omega_x \omega_z + \frac{M_y}{J_y} \\ \dot{\omega}_z = \frac{J_x - J_y}{J_z} \omega_x \omega_y + \frac{M_z}{J_z} \end{cases} \quad (5)$$

where ω_x , ω_y , and ω_z respectively denote body-axis roll, yaw, and pitch angular rates; J_x , J_y , and J_z respectively denote roll, yaw, and pitch moments of inertia; M_x , M_y , and M_z respectively denote roll, yaw, and pitch moments.

The aerodynamic forces are defined in the velocity coordinate system. The aerodynamic moments are defined in the missile body coordinate system. The aerodynamic forces and

aerodynamic moments are described by

$$\begin{cases} Y = C_Y^\alpha qS\alpha + d_Y \\ Z = C_Z^\beta qS\beta + d_Z \end{cases} \quad (6)$$

$$\begin{cases} M_x = (m_x^\alpha \alpha + m_x^\beta \beta + m_x^{\delta_x} \delta_x) qSL + d_{M_x} \\ M_y = (m_y^\beta \beta + m_y^{\delta_y} \delta_y) qSL + d_{M_y} \\ M_z = (m_z^\alpha \alpha + m_z^{\delta_z} \delta_z) qSL + d_{M_z} \end{cases} \quad (7)$$

where δ_x , δ_y , and δ_z respectively denote aileron, rudder, and elevator deflections; C_Y^α and C_Z^β denote corresponding aerodynamic force coefficients; m_x^α , m_x^β , $m_x^{\delta_x}$, m_y^β , $m_y^{\delta_y}$, m_z^α , and $m_z^{\delta_z}$ denote corresponding aerodynamic moment coefficients; S is reference area; L is reference length; q is dynamic pressure; d_Y , d_Z , d_{M_x} , d_{M_y} , and d_{M_z} are the aerodynamic modeling errors.

In order to simplify the IGC model, we make the following assumption

Assumption 1: Assuming that STT missile maintain the velocity deflection angle γ_v near zero throughout the engagement. Therefore, we have $\sin \gamma_v \approx 0$, $\cos \gamma_v \approx 1$.

According to the above analysis, the 3-D IGC model can be formulated as the following state-space expression with strict feedback form

$$\begin{cases} \dot{\mathbf{x}}_0 = \mathbf{f}_0(\mathbf{x}_0) + \mathbf{g}_0(\mathbf{x}_0) \mathbf{x}_1^* + \mathbf{d}_0 \\ \dot{\mathbf{x}}_1 = \mathbf{f}_1(\mathbf{x}_1) + \mathbf{g}_1(\mathbf{x}_1) \mathbf{x}_2 + \mathbf{d}_1 \\ \dot{\mathbf{x}}_2 = \mathbf{f}_2(\mathbf{x}_1, \mathbf{x}_2) + \mathbf{g}_2(\mathbf{x}_2) \mathbf{u} + \mathbf{d}_2 \end{cases} \quad (8)$$

where the state vectors are shown as $\mathbf{x}_0 = [\dot{q}_1 \ \dot{q}_2]^T$, $\mathbf{x}_1^* = [\alpha \ \beta]^T$, $\mathbf{x}_1 = [\alpha \ \beta \ \gamma_v]^T$, $\mathbf{x}_2 = [\omega_x \ \omega_y \ \omega_z]^T$, $\mathbf{u} = [\delta_x \ \delta_y \ \delta_z]^T$, \mathbf{d}_0 , \mathbf{d}_1 , and \mathbf{d}_2 are the system uncertainty terms, including modeling errors, aerodynamic coefficient uncertainties, and the external disturbances. Moreover, the nonlinear functions are shown as

$$\begin{aligned} \mathbf{f}_0(\mathbf{x}_0) &= \begin{bmatrix} -\frac{2\dot{R}}{R} \dot{q}_1 - \frac{\sin(2q_1)}{2} \dot{q}_2^2 + \frac{f_q}{R} g \cos \theta \\ -\frac{2\dot{R}}{R} \dot{q}_2 + 2\dot{q}_1 \dot{q}_2 \tan q_1 + \frac{\sin(2\theta) \sin(q_2 - \phi_c)}{2R \cos q_1} g \end{bmatrix}, \\ \mathbf{g}_0(\mathbf{x}_0) &= \begin{bmatrix} -\frac{f_q}{mR} C_Y^\alpha qS & -\frac{\sin q_1 \sin(q_2 - \phi_c)}{mR} C_Z^\beta qS \\ -\frac{\sin \theta \sin(q_2 - \phi_c)}{mR \cos q_1} C_Y^\alpha qS & \frac{\cos(q_2 - \phi_c)}{mR \cos q_1} C_Z^\beta qS \end{bmatrix}, \end{aligned}$$

$$\mathbf{f}_1(\mathbf{x}_1) = \begin{bmatrix} -\frac{\alpha}{mV_m \cos \beta} C_Y^\alpha qS + \frac{g}{V_m \cos \beta} \cos \theta \cos \gamma_v \\ \frac{\beta}{mV_m} C_Z^\beta qS + \frac{g}{V_m} \cos \theta \sin \gamma_v \\ -m \cos \theta \cos \gamma_v \tan \beta + C_Z^\beta qS \beta \tan \theta \cos \gamma_v \\ \frac{mV_m}{mV_m} C_Y^\alpha qS \alpha (\tan \theta \sin \gamma_v + \tan \beta) + \frac{g}{mV_m} \end{bmatrix},$$

$$\mathbf{f}_2(\mathbf{x}_1, \mathbf{x}_2) = \begin{bmatrix} \frac{J_y - J_z}{J_x} \omega_z \omega_y + \frac{(m_x^\alpha \alpha + m_x^\beta \beta) qSL}{J_x} \\ \frac{J_z - J_x}{J_y} \omega_x \omega_z + \frac{m_y^\beta \beta qSL}{J_y} \\ \frac{J_x - J_y}{J_z} \omega_y \omega_x + \frac{m_z^\alpha \alpha qSL}{J_z} \end{bmatrix},$$

$$\mathbf{g}_1(\mathbf{x}_1) = \begin{bmatrix} -\cos \alpha \tan \beta & \sin \alpha \tan \beta & 1 \\ \sin \alpha & \cos \alpha & 0 \\ \cos \alpha \sec \beta & -\sin \alpha \sec \beta & 0 \end{bmatrix},$$

$$\mathbf{g}_2(\mathbf{x}_2) = qSL \begin{bmatrix} \frac{m_x^{\delta_x}}{J_x} & 0 & 0 \\ 0 & \frac{m_y^{\delta_y}}{J_y} & 0 \\ 0 & 0 & \frac{m_z^{\delta_z}}{J_z} \end{bmatrix}.$$

The following lemmas will be used in the subsequent IGC law development and analysis.

Lemma 1 (See [36]): Consider the nonlinear system $\dot{\mathbf{x}} = \mathbf{f}(\mathbf{x}, t)$, $\mathbf{x} \in \mathbf{R}^n$. Assuming that $V(\mathbf{x})$ is a continuous and positive definite function and satisfies the differential inequality

$$\dot{V}(\mathbf{x}) \leq -\mu V(\mathbf{x}) - \eta V^\sigma(\mathbf{x}) \quad (9)$$

where μ , η , and $0 < \sigma < 1$ are positive constants. $\mathbf{x}(t_0) = \mathbf{x}_0$, and t_0 is the initial time. Then, the time of system states arriving at the equilibrium point T satisfies the following inequality

$$T \leq \frac{1}{\mu(1-\sigma)} \ln \frac{\mu V^{1-\sigma}(\mathbf{x}_0) + \eta}{\eta} \quad (10)$$

That is, the system states are finite-time convergent.

Lemma 2 (See [36]): Suppose $a_1, a_2, \dots, a_n \in \mathbf{R}$ and $0 < \kappa < 2$ are all positive constants, then the following inequality holds

$$(a_1^2 + a_2^2 + \dots + a_n^2)^\kappa \leq (a_1^\kappa + a_2^\kappa + \dots + a_n^\kappa)^2 \quad (11)$$

III. DESIGN OF 3-D INTEGRATED GUIDANCE AND CONTROL LAW

In this section, we develop a novel IGC law based on the nonsingular FITSMC and the ESO for the uncertain nonlinear system (8). And stability analysis is also presented based on Lyapunov theory.

The design objective is to establish the IGC law such that the LOS angular rates \dot{q}_1 and \dot{q}_2 will converge to zero, and the LOS angles q_1 and q_2 will converge to the desired LOS angles q_{1f} and q_{2f} .

A. NONSINGULAR FITSMC DESIGN

The tracking error states are defined as

$$e_0 = \mathbf{x}_0 + \mathbf{C} \left(\begin{bmatrix} q_1 & q_2 \end{bmatrix}^T - \begin{bmatrix} q_{1f} & q_{2f} \end{bmatrix}^T \right) \quad (12)$$

$$e_i = \mathbf{x}_i - \mathbf{x}_{ic}, \quad i = 1, 2 \quad (13)$$

where $\mathbf{C} = \text{diag}(C_1, C_2)$, C_1 and C_2 are positive constants.

Three fractional integral terminal sliding surfaces are defined as

$$S_i = \text{sgn}^{p_{1i}/p_{2i}}(e_i) + \alpha_i \int_0^t (e_i + \beta_i \text{sgn}^{p_{1i}/p_{2i}}(e_i)) dt, \quad i = 0, 1, 2 \quad (14)$$

where $\text{sgn}^\delta(\mathbf{y}) = [|y_1|^\delta \text{sgn}(y_1) \cdots |y_n|^\delta \text{sgn}(y_n)]^T$, $\mathbf{y} \in \mathbf{R}^n$, $\delta > 0$; $\alpha_i > 0$, $\beta_i > 1$; p_{1i} and p_{2i} are positive odd constants, and $1 < p_{1i}/p_{2i} < 2$.

Remark 1: The FITSMC scheme aims at steering tracking error states to small neighborhood of zero in finite-time and avoiding the singularity problem in the IGC law design.

B. IGC LAW DESIGN BASED ON NONSINGULAR FITSMC FOR MISSILES

The following assumption will be used for controller design and performance analysis.

Assumption 2: All the control gain matrices of system (8) are nonsingular and norm-bounded.

The design of IGC law is elaborated as follows:

Step 1: The time derivative of S_0 is given by

$$\begin{aligned} \dot{S}_0 &= \frac{p_{10}}{p_{20}} \text{diag} |e_0|^{p_{10}/p_{20}-1} \dot{e}_0 + \alpha_0 (e_0 + \beta_0 \text{sgn}^{p_{10}/p_{20}}(e_0)) \\ &= \frac{p_{10}}{p_{20}} \text{diag} |e_0|^{p_{10}/p_{20}-1} (\mathbf{f}_0(\mathbf{x}_0) + \mathbf{g}_0(\mathbf{x}_0) \mathbf{x}_1^* + \mathbf{d}_0 + \mathbf{C}\mathbf{x}_0) \\ &\quad + \alpha_0 (e_0 + \beta_0 \text{sgn}^{p_{10}/p_{20}}(e_0)) \end{aligned} \quad (15)$$

where $\text{diag} |y|^\delta = \text{diag} (|y_1|^\delta, \dots, |y_n|^\delta)$, $\mathbf{y} \in \mathbf{R}^n$, $\delta > 0$.

Constructing the following ESO to estimate the disturbance \mathbf{d}_0

$$\begin{cases} \mathbf{e}_{z0} = \mathbf{x}_0 - \mathbf{z}_{10} \\ \dot{\mathbf{z}}_{10} = \mathbf{f}_0(\mathbf{z}_{10}) + \mathbf{g}_0(\mathbf{z}_{10}) \mathbf{x}_1^* + \mathbf{z}_{20} + h_{10} \text{sgmf}(\mathbf{e}_{z0}) \\ \quad + \beta_{10} (\text{sgn}^{m_1}(\mathbf{e}_{z0}) + \text{sgn}^{m_2}(\mathbf{e}_{z0})) \\ \dot{\mathbf{z}}_{20} = \beta_{20} (\text{sgn}^{n_1}(\mathbf{e}_{z0}) + \text{sgn}^{n_2}(\mathbf{e}_{z0})) + h_{20} \text{sgmf}(\mathbf{e}_{z0}) \end{cases} \quad (16)$$

where $0.5 < m_1 < 1$, $m_2 = 1/m_1$, $n_1 = 2m_1 - 1$, and $n_2 = 1/m_2 + m_2 - 1$; $\beta_{10} > 0$ and $\beta_{20} = \beta_{10}^2$ are the gains of ESO, h_{10} and h_{20} are positive constants. $\text{sgmf}(\mathbf{y}) = [\text{sgmf}(y_1) \cdots \text{sgmf}(y_n)]^T$, $\mathbf{y} \in \mathbf{R}^n$, $\text{sgmf}(y_i)$ is the sigmoid function and is of the form

$$\text{sgmf}(y_i) = \begin{cases} 2 \left(\frac{1}{1+e^{-\tau y_i}} - \frac{1}{2} \right), & |y_i| \leq \chi \\ \text{sgn}(y_i), & |y_i| > \chi, \end{cases}$$

τ and χ are positive constants.

One gets the virtual control law \mathbf{x}_{1d}^* as

$$\mathbf{x}_{1d}^* = -\mathbf{g}_0(\mathbf{x}_0)^{-1} \begin{bmatrix} w_0 \mathbf{S}_0 + \mathbf{f}_0(\mathbf{x}_0) + \mathbf{C}\mathbf{x}_0 + \mathbf{z}_{20} \\ + k_0 \text{sgn}^\rho(\mathbf{S}_0) + \frac{p_{20}}{p_{10}} \text{diag} |e_0|^{2-p_{10}/p_{20}} \\ \times \alpha_0 (\mathbf{I} + \beta_0 \text{diag} |e_0|^{p_{10}/p_{20}-1}) \text{sgn}(\mathbf{e}_0) \end{bmatrix} \quad (17)$$

where $0 < \rho < 1$, w_0 and k_0 are positive constants.

In order to address the problem of ‘‘explosion of terms’’ and achieve finite-time convergence, a modified filter is designed to handle the virtual control law. \mathbf{x}_{1d}^* passes through the following modified filter to yield the virtual control law \mathbf{x}_{1c}^* . Define $\boldsymbol{\rho}_1^* = \mathbf{x}_{1c}^* - \mathbf{x}_{1d}^*$, and this modified filter is designed as

$$\tau_1 \dot{\mathbf{x}}_{1c}^* + \mathbf{x}_{1c}^* = \mathbf{x}_{1d}^* - r_1 \text{sgn}^\rho(\boldsymbol{\rho}_1^*), \quad \mathbf{x}_{1c}^*(0) = \mathbf{x}_{1d}^*(0) \quad (18)$$

where τ_1 and r_1 are positive constants.

For STT missile, the velocity deflection angle γ_v should be maintained near zero throughout the engagement. So we have

$$\mathbf{x}_{1d} = \begin{bmatrix} \mathbf{x}_{1d}^{*T} & 0 \end{bmatrix}^T, \quad \mathbf{x}_{1c} = \begin{bmatrix} \mathbf{x}_{1c}^{*T} & 0 \end{bmatrix}^T \quad (19)$$

Step 2: The time derivative of S_1 is given by

$$\begin{aligned} \dot{S}_1 &= \frac{p_{11}}{p_{21}} \text{diag} |e_1|^{p_{11}/p_{21}-1} \dot{e}_1 + \alpha_1 (e_1 + \beta_1 \text{sgn}^{p_{11}/p_{21}}(e_1)) \\ &= \frac{p_{11}}{p_{21}} \text{diag} |e_1|^{p_{11}/p_{21}-1} (\mathbf{f}_1(\mathbf{x}_1) + \mathbf{g}_1(\mathbf{x}_1) \mathbf{x}_2 + \mathbf{d}_1 - \dot{\mathbf{x}}_{1c}) \\ &\quad + \alpha_1 (e_1 + \beta_1 \text{sgn}^{p_{11}/p_{21}}(e_1)) \end{aligned} \quad (20)$$

Constructing the following ESO to estimate the disturbance \mathbf{d}_1

$$\begin{cases} \mathbf{e}_{z1} = \mathbf{x}_1 - \mathbf{z}_{11} \\ \dot{\mathbf{z}}_{11} = \mathbf{f}_1(\mathbf{z}_{11}) + \mathbf{g}_1(\mathbf{z}_{11}) \mathbf{x}_2 + h_{11} \text{sgmf}(\mathbf{e}_{z1}) + \mathbf{z}_{21} \\ \quad + \beta_{11} (\text{sgn}^{m_1}(\mathbf{e}_{z1}) + \text{sgn}^{m_2}(\mathbf{e}_{z1})) \\ \dot{\mathbf{z}}_{21} = \beta_{21} (\text{sgn}^{n_1}(\mathbf{e}_{z1}) + \text{sgn}^{n_2}(\mathbf{e}_{z1})) + h_{21} \text{sgmf}(\mathbf{e}_{z1}) \end{cases} \quad (21)$$

where $\beta_{11} > 0$ and $\beta_{21} = \beta_{11}^2$ are the gains of ESO, h_{11} and h_{21} are positive constants.

One gets the virtual control law \mathbf{x}_{2d} as

$$\mathbf{x}_{2d} = -\mathbf{g}_1(\mathbf{x}_1)^{-1} \begin{bmatrix} w_1 \mathbf{S}_1 + \mathbf{f}_1(\mathbf{x}_1) - \dot{\mathbf{x}}_{1c} + \mathbf{z}_{21} \\ + k_1 \text{sgn}^\rho(\mathbf{S}_1) + \frac{p_{21}}{p_{11}} \text{diag} |e_1|^{2-p_{11}/p_{21}} \\ \times \alpha_1 (\mathbf{I} + \beta_1 \text{diag} |e_1|^{p_{11}/p_{21}-1}) \text{sgn}(\mathbf{e}_1) \end{bmatrix} \quad (22)$$

where w_1 and k_1 are positive constants.

Let \mathbf{x}_{2d} passes through the following modified filter to yield the virtual control law \mathbf{x}_{2c} . Define $\boldsymbol{\rho}_2 = \mathbf{x}_{2c} - \mathbf{x}_{2d}$, and the modified filter is designed as

$$\tau_2 \dot{\mathbf{x}}_{2c} + \mathbf{x}_{2c} = \mathbf{x}_{2d} - r_2 \text{sgn}^\rho(\boldsymbol{\rho}_2), \quad \mathbf{x}_{2c}(0) = \mathbf{x}_{2d}(0) \quad (23)$$

where τ_2 and r_2 are positive constants.

Step 3: The time derivative of S_2 is given by

$$\begin{aligned} \dot{S}_2 &= \frac{p_{12}}{p_{22}} \text{diag} |e_2|^{p_{12}/p_{22}-1} \dot{e}_2 + \alpha_2 (e_2 + \beta_2 \text{sgn}^{p_{12}/p_{22}}(e_2)) \\ &= \frac{p_{12}}{p_{22}} \text{diag} |e_2|^{p_{12}/p_{22}-1} (f_2(x_1, x_2) + g_2(x_2)u + d_2 - \dot{x}_{2c}) \\ &\quad + \alpha_2 (e_2 + \beta_2 \text{sgn}^{p_{12}/p_{22}}(e_2)) \end{aligned} \quad (24)$$

Constructing the following ESO to estimate the disturbance d_2

$$\begin{cases} \dot{e}_{z2} = x_2 - z_{12} \\ \dot{z}_{12} = f_2(z_{11}, z_{12}) + g_2(z_{12})u + h_{12} \text{sgmf}(e_{z2}) + z_{22} \\ \quad + \beta_{12} (\text{sgn}^{m_1}(e_{z2}) + \text{sgn}^{m_2}(e_{z2})) \\ \dot{z}_{22} = \beta_{22} (\text{sgn}^{n_1}(e_{z2}) + \text{sgn}^{n_2}(e_{z2})) + h_{22} \text{sgmf}(e_{z2}) \end{cases} \quad (25)$$

where $\beta_{12} > 0$ and $\beta_{22} = \beta_{12}^2$ are the gains of ESO, h_{12} and h_{22} are positive constants.

Then, a novel IGC law u for missile intercepting maneuvering target with impact angle constraint is defined as

$$u = -g_2(x_2)^{-1} \begin{bmatrix} w_2 S_2 + f_2(x_1, x_2) - \dot{x}_{2c} + z_{22} \\ + k_2 \text{sgn}^\rho(S_2) + \frac{p_{22}}{p_{12}} \text{diag} |e_2|^{2-p_{12}/p_{22}} \\ \times \alpha_2 (\mathbf{I} + \beta_2 \text{diag} |e_2|^{p_{12}/p_{22}-1}) \text{sgn}(e_2) \end{bmatrix} \quad (26)$$

where w_2 and k_2 are positive constants.

C. STABILITY ANALYSIS OF IGC SYSTEM

Before investigation on stability analysis, the following assumption is introduced.

Assumption 3: The estimation errors of d_0 , d_1 , and d_2 are norm-bounded. E_i , $i = 0, 1, 2$ are selected to satisfy $\|z_{2i} - d_i\| \leq E_i$.

Theorem 1: Consider the IGC system (8) under Assumption 2 and 3, the IGC law u is designed as (26). If the sliding surfaces are designed as (14), and the errors of filter are defined as (27), then the sliding surface variables and the errors of filter will converge to the regions as (48)-(50) in finite time.

Proof: For convenience, a function $f(\cdot)$ will be denoted as f in the subsequent process.

Define the errors of low-pass filters as

$$\rho_i = x_{ic} - x_{id}, \quad i = 1, 2 \quad (27)$$

From (18) and (19), it can be obtained that

$$\tau_1 \dot{x}_{1c} + x_{1c} = x_{1d} - r_1 \text{sgn}^\rho(\rho_1), \quad x_{1c}(0) = x_{1d}(0) \quad (28)$$

Derivative of ρ_i can be derived as

$$\begin{aligned} \dot{\rho}_i &= \dot{x}_{ic} - \dot{x}_{id} \\ &= -\tau_i^{-1} \rho_i - \tau_i^{-1} r_i \text{sgn}^\rho(\rho_i) - \dot{x}_{id} \end{aligned} \quad (29)$$

As pointed out in [31], the derivatives of x_{id} exist and are norm bounded.

Define the following Lyapunov function candidate as

$$V_{\rho_i} = \frac{1}{2} \rho_i^T \rho_i \quad (30)$$

Taking the time derivative of V_{ρ_i} and using Lemma 2 give

$$\begin{aligned} \dot{V}_{\rho_i} &= \rho_i^T \dot{\rho}_i = \rho_i^T \left(-\tau_i^{-1} \rho_i - \tau_i^{-1} r_i \text{sgn}^\rho(\rho_i) - \dot{x}_{id} \right) \\ &= -\tau_i^{-1} \rho_i^T \rho_i - \tau_i^{-1} r_i \rho_i^T \text{sgn}^\rho(\rho_i) - \rho_i^T \dot{x}_{id} \\ &\leq -\tau_i^{-1} \rho_i^T \rho_i - \tau_i^{-1} r_i \|\rho_i\|^{\rho+1} + \|\rho_i\| \|\dot{x}_{id}\| \end{aligned} \quad (31)$$

Define the state tracking errors as (14), differentiating them with respect to time along (17), (22), and (28) yield

$$\begin{aligned} \dot{S}_0 &= \frac{p_{10}}{p_{20}} \text{diag} |e_0|^{p_{10}/p_{20}-1} (f_0 + Cx_0 + g_0 x_1^* + d_0) \\ &\quad + \alpha_0 (e_0 + \beta_0 \text{sgn}^{p_{10}/p_{20}}(e_0)) \\ &= \frac{p_{10}}{p_{20}} \text{diag} |e_0|^{p_{10}/p_{20}-1} [-w_0 S_0 - z_{20} - k_0 \text{sgn}^\rho(S_0) \\ &\quad + d_0 + g_0 (\rho_1^* + e_1^*)] \end{aligned} \quad (32)$$

where $e_1^* = x_1^* - x_{1c}^*$.

$$\begin{aligned} \dot{S}_1 &= \frac{p_{11}}{p_{21}} \text{diag} |e_1|^{p_{11}/p_{21}-1} (f_1 + g_1 x_2 + d_1 - \dot{x}_{1c}) \\ &\quad + \alpha_1 (e_1 + \beta_1 \text{sgn}^{p_{11}/p_{21}}(e_1)) \\ &= \frac{p_{11}}{p_{21}} \text{diag} |e_1|^{p_{11}/p_{21}-1} [-w_1 S_1 - z_{21} - k_1 \text{sgn}^\rho(S_1) \\ &\quad + d_1 + g_1 (\rho_2 + e_2)] \end{aligned} \quad (33)$$

$$\begin{aligned} \dot{S}_2 &= \frac{p_{12}}{p_{22}} \text{diag} |e_2|^{p_{12}/p_{22}-1} (f_2 + g_2 u + d_2 - \dot{x}_{2c}) \\ &\quad + \alpha_2 (e_2 + \beta_2 \text{sgn}^{p_{12}/p_{22}}(e_2)) \\ &= \frac{p_{12}}{p_{22}} \text{diag} |e_2|^{p_{12}/p_{22}-1} [-w_2 S_2 - z_{22} - k_2 \text{sgn}^\rho(S_2) + d_2] \end{aligned} \quad (34)$$

Choose the Lyapunov function candidate as

$$V_{S_i} = \frac{1}{2} S_i^T S_i \quad (35)$$

Evaluating the time derivative of V_{S_i} and using Lemma 2 give

$$\begin{aligned} \dot{V}_{S_0} &= S_0^T \dot{S}_0 \\ &= \frac{p_{10}}{p_{20}} S_0^T \text{diag} |e_0|^{p_{10}/p_{20}-1} [-w_0 S_0 - (z_{20} - d_0) \\ &\quad - k_0 \text{sgn}^\rho(S_0) + g_0 (\rho_1^* + e_1^*)] \\ &\leq \frac{p_{10}}{p_{20}} \left[-w_0 b_0 S_0^T S_0 + \|S_0\| \|z_{20} - d_0\| \right. \\ &\quad \times \left\| \text{diag} |e_0|^{p_{10}/p_{20}-1} \right\| - k_0 b_0 \|S_0\|^{\rho+1} + \frac{1}{2} \rho_1^T \rho_1 \\ &\quad + \|S_0\| \|g_0\| \|e_1\| \left\| \text{diag} |e_0|^{p_{10}/p_{20}-1} \right\| \\ &\quad \left. + \frac{1}{2} S_0^T \text{diag} |e_0|^{p_{10}/p_{20}-1} g_0 g_0^T \right. \\ &\quad \left. \times \left(\text{diag} |e_0|^{p_{10}/p_{20}-1} \right)^T S_0 \right] \\ &\leq \frac{p_{10}}{p_{20}} \left[- \left(w_0 b_0 - \frac{1}{2} c_0^2 \|g_0\|^2 \right) S_0^T S_0 - k_0 b_0 \|S_0\|^{\rho+1} \right. \\ &\quad \left. + c_0 (E_0 + \|g_0\| \|e_1\|) \|S_0\| + \frac{1}{2} \rho_1^T \rho_1 \right] \end{aligned} \quad (36)$$

where $b_0 = \min \{ |e_{01}|^{p_{10}/p_{20}-1}, |e_{02}|^{p_{10}/p_{20}-1} \}$,

$$\begin{aligned}
 c_0 &= \left\| \text{diag } |e_0|^{p_{10}/p_{20}-1} \right\|. \\
 \dot{V}_{S_1} &= S_1^T \dot{S}_1 \\
 &= \frac{p_{11}}{p_{21}} S_1^T \text{diag } |e_1|^{p_{11}/p_{21}-1} [-w_1 S_1 - (z_{21} - d_1) \\
 &\quad - k_1 \text{sgn}^\rho(S_1) + g_1(\rho_2 + e_2)] \\
 &\leq \frac{p_{11}}{p_{21}} \left[-w_1 b_1 S_1^T S_1 + \|S_1\| \|g_1\| \|e_2\| \right. \\
 &\quad \times \left\| \text{diag } |e_1|^{p_{11}/p_{21}-1} \right\| - k_1 b_1 \|S_1\|^{\rho+1} + \frac{1}{2} \rho_2^T \rho_2 \\
 &\quad + \|S_1\| \|z_{21} - d_1\| \left\| \text{diag } |e_1|^{p_{11}/p_{21}-1} \right\| \\
 &\quad + \frac{1}{2} S_1^T \text{diag } |e_1|^{p_{11}/p_{21}-1} g_1 g_1^T \\
 &\quad \left. \times \left(\text{diag } |e_1|^{p_{11}/p_{21}-1} \right)^T S_1 \right] \\
 &\leq \frac{p_{11}}{p_{21}} \left[- \left(w_1 b_1 - \frac{1}{2} c_1^2 \|g_1\|^2 \right) S_1^T S_1 - k_1 b_1 \|S_1\|^{\rho+1} \right. \\
 &\quad \left. + c_1 (E_1 + \|g_1\| \|e_2\|) \|S_1\| + \frac{1}{2} \rho_2^T \rho_2 \right] \quad (37)
 \end{aligned}$$

where $b_1 = \min \{ |e_{11}|^{p_{11}/p_{21}-1}, |e_{12}|^{p_{11}/p_{21}-1}, |e_{13}|^{p_{11}/p_{21}-1} \}$, $c_1 = \left\| \text{diag } |e_1|^{p_{11}/p_{21}-1} \right\|$.

$$\begin{aligned}
 \dot{V}_{S_2} &= S_2^T \dot{S}_2 = \frac{p_{12}}{p_{22}} S_2^T \text{diag } |e_2|^{p_{12}/p_{22}-1} [-w_2 S_2 \\
 &\quad - (z_{22} - d_2) - k_2 \text{sgn}^\rho(S_2)] \\
 &\leq \frac{p_{12}}{p_{22}} \left[-w_2 b_2 S_2^T S_2 - k_2 b_2 \|S_2\|^{\rho+1} \right. \\
 &\quad \left. + \|S_2\| \|z_{22} - d_2\| \left\| \text{diag } |e_2|^{p_{12}/p_{22}-1} \right\| \right] \\
 &\leq \frac{p_{12}}{p_{22}} \left[-w_2 b_2 S_2^T S_2 - k_2 b_2 \|S_2\|^{\rho+1} + c_2 E_2 \|S_2\| \right] \quad (38)
 \end{aligned}$$

where $b_2 = \min \{ |e_{21}|^{p_{12}/p_{22}-1}, |e_{22}|^{p_{12}/p_{22}-1}, |e_{23}|^{p_{12}/p_{22}-1} \}$, $c_2 = \left\| \text{diag } |e_2|^{p_{12}/p_{22}-1} \right\|$.

Consider the following Lyapunov function candidate as

$$V = \sum_{i=1}^2 V_{\rho_i} + \sum_{i=0}^2 V_{S_i} \quad (39)$$

Differentiating V with respect to time along (31), (36), (37), and (38) give

$$\begin{aligned}
 \dot{V} &= \dot{V}_{\rho_1} + \dot{V}_{\rho_2} + \dot{V}_{S_0} + \dot{V}_{S_1} + \dot{V}_{S_2} \\
 &\leq -\tau_1^{-1} \rho_1^T \rho_1 - \tau_1^{-1} r_1 \| \rho_1 \| \rho_1^{\rho+1} + \| \rho_1 \| \| \dot{x}_{1d} \| - \tau_2^{-1} \rho_2^T \rho_2 \\
 &\quad - \tau_2^{-1} r_2 \| \rho_2 \| \rho_2^{\rho+1} + \| \rho_2 \| \| \dot{x}_{2d} \| \\
 &\quad + \frac{p_{10}}{p_{20}} \left[- \left(w_0 b_0 - \frac{1}{2} c_0^2 \|g_0\|^2 \right) S_0^T S_0 - k_0 b_0 \|S_0\|^{\rho+1} \right. \\
 &\quad \left. + c_0 (E_0 + \|g_0\| \|e_1\|) \|S_0\| + \frac{1}{2} \rho_1^T \rho_1 \right] \\
 &\quad + \frac{p_{11}}{p_{21}} \left[- \left(w_1 b_1 - \frac{1}{2} c_1^2 \|g_1\|^2 \right) S_1^T S_1 - k_1 b_1 \|S_1\|^{\rho+1} \right.
 \end{aligned}$$

$$\begin{aligned}
 &\quad \left. + c_1 (E_1 + \|g_1\| \|e_2\|) \|S_1\| + \frac{1}{2} \rho_2^T \rho_2 \right] \\
 &\quad + \frac{p_{12}}{p_{22}} \left[-w_2 b_2 S_2^T S_2 - k_2 b_2 \|S_2\|^{\rho+1} + c_2 E_2 \|S_2\| \right] \\
 &\leq \sum_{i=1}^2 \left[- \left(\tau_i^{-1} - \frac{1}{2} \frac{p_{1i-1}}{p_{2i-1}} \right) \rho_i^T \rho_i - \tau_i^{-1} r_i \| \rho_i \| \rho_i^{\rho+1} \right. \\
 &\quad \left. + \| \rho_i \| \| \dot{x}_{id} \| \right] + \sum_{i=0}^1 \frac{p_{1i}}{p_{2i}} \left[- \left(w_i b_i - \frac{1}{2} c_i^2 \|g_i\|^2 \right) \right. \\
 &\quad \left. S_i^T S_i - k_i b_i \|S_i\|^{\rho+1} + c_i (E_i + \|g_i\| \|e_{i+1}\|) \|S_i\| \right] \\
 &\quad + \frac{p_{12}}{p_{22}} \left[-w_2 b_2 S_2^T S_2 - k_2 b_2 \|S_2\|^{\rho+1} + c_2 E_2 \|S_2\| \right] \quad (40)
 \end{aligned}$$

which can be further changed into the following two forms

$$\begin{aligned}
 \dot{V} &\leq \sum_{i=1}^2 \left[- \left(\tau_i^{-1} - \frac{1}{2} \frac{p_{1i-1}}{p_{2i-1}} - \frac{\| \dot{x}_{id} \|}{\| \rho_i \|} \right) \rho_i^T \rho_i \right. \\
 &\quad \left. - \tau_i^{-1} r_i \| \rho_i \| \rho_i^{\rho+1} \right] \\
 &\quad + \sum_{i=0}^1 \frac{p_{1i}}{p_{2i}} \left[- \left(w_i b_i - \frac{1}{2} c_i^2 \|g_i\|^2 \right. \right. \\
 &\quad \left. \left. - \frac{E_i + \|g_i\| \|e_{i+1}\|}{\|S_i\|} c_i \right) S_i^T S_i - k_i b_i \|S_i\|^{\rho+1} \right] \\
 &\quad + \frac{p_{12}}{p_{22}} \left[- \left(w_2 b_2 - \frac{c_2 E_2}{\|S_2\|} \right) S_2^T S_2 - k_2 b_2 \|S_2\|^{\rho+1} \right] \quad (41)
 \end{aligned}$$

And

$$\begin{aligned}
 \dot{V} &\leq \sum_{i=1}^2 \left[- \left(\tau_i^{-1} - \frac{1}{2} \frac{p_{1i-1}}{p_{2i-1}} \right) \rho_i^T \rho_i \right. \\
 &\quad \left. - \left(\tau_i^{-1} r_i - \frac{\| \dot{x}_{id} \|}{\| \rho_i \|} \right) \| \rho_i \| \rho_i^{\rho+1} \right] \\
 &\quad + \sum_{i=0}^1 \frac{p_{1i}}{p_{2i}} \left[- \left(w_i b_i - \frac{1}{2} c_i^2 \|g_i\|^2 \right) S_i^T S_i \right. \\
 &\quad \left. - \left(k_i b_i - \frac{E_i + \|g_i\| \|e_{i+1}\|}{\|S_i\|} c_i \right) \|S_i\|^{\rho+1} \right] \\
 &\quad + \frac{p_{12}}{p_{22}} \left[-w_2 b_2 S_2^T S_2 - \left(k_2 b_2 - \frac{c_2 E_2}{\|S_2\|} \right) \|S_2\|^{\rho+1} \right] \quad (42)
 \end{aligned}$$

For (41), when

$$\begin{cases} \lambda_{1i} = \tau_i^{-1} - \frac{1}{2} \frac{p_{1i-1}}{p_{2i-1}} - \frac{\| \dot{x}_{id} \|}{\| \rho_i \|} > 0, & i = 1, 2 \\ \lambda_{2i} = w_i b_i - \frac{1}{2} c_i^2 \|g_i\|^2 - \frac{E_i + \|g_i\| \|e_{i+1}\|}{\|S_i\|} c_i > 0, & i = 0, 1 \\ \lambda_{22} = w_2 b_2 - \frac{c_2 E_2}{\|S_2\|} > 0 \end{cases} \quad (43)$$

Then, one can obtain

$$\begin{aligned} \dot{V} &\leq \sum_{i=1}^2 \left[-\lambda_{1i} \rho_i^T \rho_i - \tau_i^{-1} r_i \|\rho_i\|^{\rho+1} \right] \\ &\quad + \sum_{i=0}^2 \frac{p_{1i}}{p_{2i}} \left[-\lambda_{2i} S_i^T S_i - k_i b_i \|S_i\|^{\rho+1} \right] \\ &\leq -\sum_{i=1}^2 2\lambda_{1i} V_{\rho_i} - \sum_{i=1}^2 2^{\frac{\rho+1}{2}} \tau_i^{-1} r_i V_{\rho_i}^{\frac{\rho+1}{2}} \\ &\quad - \sum_{i=0}^2 2\lambda_{2i} \frac{p_{1i}}{p_{2i}} V_{S_i} - \sum_{i=0}^2 2^{\frac{\rho+1}{2}} k_i b_i \frac{p_{1i}}{p_{2i}} V_{S_i}^{\frac{\rho+1}{2}} \\ &\leq -\varphi_1 V - \varphi_2 V^{\frac{\rho+1}{2}} \end{aligned} \tag{44}$$

where $\varphi_1 = 2 \min \left\{ \lambda_{11}, \lambda_{12}, \frac{p_{10}}{p_{20}} \lambda_{20}, \frac{p_{11}}{p_{21}} \lambda_{21}, \frac{p_{12}}{p_{22}} \lambda_{22} \right\}$, $\varphi_2 = 2^{\frac{\rho+1}{2}} \min \left\{ \tau_1^{-1} r_1, \tau_2^{-1} r_2, k_0 b_0 \frac{p_{10}}{p_{20}}, k_1 b_1 \frac{p_{11}}{p_{21}}, k_2 b_2 \frac{p_{12}}{p_{22}} \right\}$.

According to Lemma 1, these regions

$$\begin{cases} \|\rho_i\| \leq \frac{\|\dot{x}_{id}\|}{\tau_i^{-1} - \frac{1}{2} \frac{p_{1i-1}}{p_{2i-1}}}, & i = 1, 2 \\ \|\mathcal{S}_i\| \leq \frac{E_i + \|\mathbf{g}_i\| \|e_{i+1}\|}{w_i b_i - \frac{1}{2} c_i^2 \|\mathbf{g}_i\|^2} c_i, & i = 0, 1 \\ \|\mathcal{S}_2\| \leq \frac{c_2 E_2}{w_2 b_2} \end{cases} \tag{45}$$

can be reached in finite time. Similarly, for (42), when

$$\begin{cases} \tau_i^{-1} - \frac{1}{2} \frac{p_{1i-1}}{p_{2i-1}} > 0, & i = 1, 2 \\ \tau_i^{-1} r_i - \frac{\|\dot{x}_{id}\|}{\|\rho_i\|^\rho} > 0, & i = 1, 2 \\ w_i b_i - \frac{1}{2} c_i^2 \|\mathbf{g}_i\|^2 > 0, & i = 0, 1 \\ k_i b_i - \frac{E_i + \|\mathbf{g}_i\| \|e_{i+1}\|}{\|\mathcal{S}_i\|^\rho} c_i > 0, & i = 0, 1 \\ k_2 b_2 - \frac{c_2 E_2}{\|\mathcal{S}_2\|^\rho} > 0 \end{cases} \tag{46}$$

These regions

$$\begin{cases} \|\rho_i\| \leq \left(\frac{\|\dot{x}_{id}\| \tau_i}{r_i} \right)^{\frac{1}{\rho}}, & i = 1, 2 \\ \|\mathcal{S}_i\| \leq \left(\frac{E_i + \|\mathbf{g}_i\| \|e_{i+1}\|}{k_i b_i} c_i \right)^{\frac{1}{\rho}}, & i = 0, 1 \\ \|\mathcal{S}_2\| \leq \left(\frac{c_2 E_2}{k_2 b_2} \right)^{\frac{1}{\rho}} \end{cases} \tag{47}$$

can also be reached in finite time. Synthesizing (45) and (47), it can be concluded that the states of the closed-loop system will converge to these regions

$$\Omega_{1i} = \left\{ \rho_i \mid \|\rho_i\| \leq \min \left\{ \frac{\|\dot{x}_{id}\|}{\tau_i^{-1} - \frac{1}{2} \frac{p_{1i-1}}{p_{2i-1}}}, \left(\frac{\|\dot{x}_{id}\| \tau_i}{r_i} \right)^{\frac{1}{\rho}} \right\}, \right. \\ \left. i = 1, 2 \right\} \tag{48}$$

$$\Omega_{2i} = \left\{ S_i \mid \|S_i\| \leq \min \left\{ \frac{E_i + \|\mathbf{g}_i\| \|e_{i+1}\|}{w_i b_i - \frac{1}{2} c_i^2 \|\mathbf{g}_i\|^2} c_i, \left(\frac{E_i + \|\mathbf{g}_i\| \|e_{i+1}\|}{k_i b_i} c_i \right)^{\frac{1}{\rho}} \right\}, i = 0, 1 \right\} \tag{49}$$

$$\Omega_{22} = \left\{ S_2 \mid \|S_2\| \leq \min \left\{ \frac{c_2 E_2}{w_2 b_2}, \left(\frac{c_2 E_2}{k_2 b_2} \right)^{\frac{1}{\rho}} \right\} \right\} \tag{50}$$

in finite time. This completes the proof.

IV. NUMERICAL SIMULATIONS

In this section, numerical simulations are implemented for a variety of scenarios to illustrate the effectiveness and performance of the proposed IGC law.

In order to verify the superiority and robustness of the proposed IGC law, two IGC design methods respectively based on block back-stepping sliding mode and ESO in [11] and the ITSMC in [37] are used for performance comparison. For simplicity, we denote the IGC law in (26) and two contrast methods as novel IGC law (NIGC), SMC-IGC law, and ITSMC-IGC law respectively.

Define $x_m = [x_m \ y_m \ z_m]^T$ to be the position vector of missile in the inertial coordinate system, and then the center-of-mass motion of missile is described by

$$\begin{cases} \dot{x}_m = V_m \cos \theta \cos \phi_c \\ \dot{y}_m = V_m \sin \theta \\ \dot{z}_m = -V_m \cos \theta \sin \phi_c \end{cases} \tag{51}$$

The states R , q_1 , and q_2 are calculated by

$$\begin{cases} R = \sqrt{(x_t - x_m)^2 + (y_t - y_m)^2 + (z_t - z_m)^2} \\ q_1 = \arctan \left(\frac{y_t - y_m}{\sqrt{(x_t - x_m)^2 + (z_t - z_m)^2}} \right) \\ q_2 = -\arctan \left(\frac{z_t - z_m}{x_t - x_m} \right) \end{cases} \tag{52}$$

where $x_t = [x_t \ y_t \ z_t]^T$ is the position of target.

In the inertial frame of reference, the initial position coordinate vector of missile is set as $x_m(0) = 3000\text{m}$, $y_m(0) = 10000\text{m}$, and $z_m(0) = 1000\text{m}$, the initial position coordinate vector of target is set as $x_t(0) = 7000\text{m}$, $y_t(0) = 0\text{m}$, and $z_t(0) = 500\text{m}$. The nominal parameters of missile body and the nominal aerodynamic coefficients are shown in Table 1.

By missile parameter perturbations into consideration, the nominal parameters of missile body in Table 1 multiply $1 + 0.2 \sin(0.2\pi t)$ to generate the actual missile parameters.

It is assumed that the blind area of the seeker is 30 meters, the control command remains unchanged when R is smaller than 30 meters. Moreover, the control surface deflections are constrained with $\pm 35\text{deg}$.

The speed, the flight path and heading angles of missile at initial time are respectively set as $V_m = 1500 \text{ m/s}$,

TABLE 1. Missile-related parameters.

Parameter	Value	Parameter	Value
m	1200kg	$m_{\beta_1}^\beta$	-27.30
S	0.43m ²	$m_{\beta_1}^{\delta_y}$	-26.60
L	0.69m	$m_{\tau_1}^\alpha$	-28.15
J_{x_1}	100kg · m ²	$m_{\tau_1}^{\delta_z}$	-27.90
J_{y_1}	5800 kg · m ²	C_Y^α	57.15
J_{z_1}	5700 kg · m ²	C_Y^β	-0.081
ρ	1.225kg/m ³	$C_Y^{\delta_y}$	5.75
$m_{\beta_1}^\alpha$	0.45	C_Z^α	0.091
$m_{\beta_1}^\beta$	-0.38	C_Z^β	-56.32
$m_{\beta_1}^{\delta_z}$	2.13	$C_Z^{\delta_z}$	-5.6

TABLE 2. Initial conditions and controller parameters.

Parameter	Value	Parameter	Value
β_{10}	10	α_1	0.5
β_{20}	100	α_2	0.5
β_{11}	10	β_0	4
β_{21}	100	β_1	4
β_{12}	10	β_2	4
β_{22}	100	p_{10}	11
h_{10}	0.05	p_{11}	11
h_{20}	1	p_{12}	11
h_{11}	0.05	p_{20}	9
h_{21}	1	p_{21}	9
h_{12}	0.05	p_{22}	9
h_{22}	1	τ_1	0.01
ρ	0.95	τ_2	0.01
m_1	0.85	r_1	0.1
α_0	0.5	r_2	0.1

$\theta(0) = -10$ deg, and $\phi_c(0) = 0$ deg. The initial conditions and controller parameters are listed in Table 2.

In order to verify the performance of the IGC law, simulation experiments are constructed under the following three cases.

Case 1: In this subsection, a STT missile is considered during its terminal guidance phase to intercept a ground maneuvering target. For the target, the initial velocity is set as $V_t(0) = 30$ m/s, the flight path and heading angles at initial time are set as $\theta_t(0) = 0$ deg and $\phi_{ct}(0) = 7$ deg. The normal and tangential accelerations of the target are set as $a_n = 5 * \sin(0.2\pi t)$ m/s² and $a_t = 5 * \sin(0.2\pi t)$ m/s². The desired impact angles are respectively set as $q_{1f} = -80$ deg and $q_{2f} = 10$ deg. The simulation results are shown in Figs. 3-8.

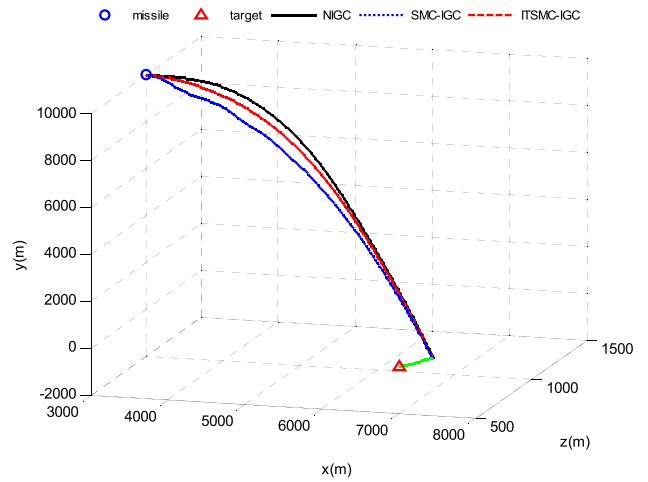


FIGURE 3. Three-dimensional trajectories of missile and target in case 1.

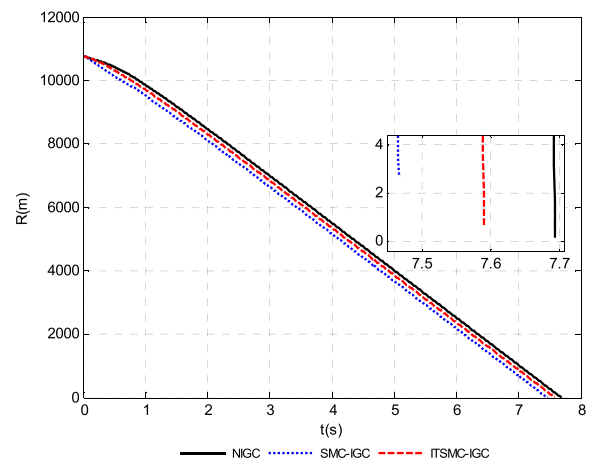


FIGURE 4. Curves of the relative distance between missile and target in case 1.

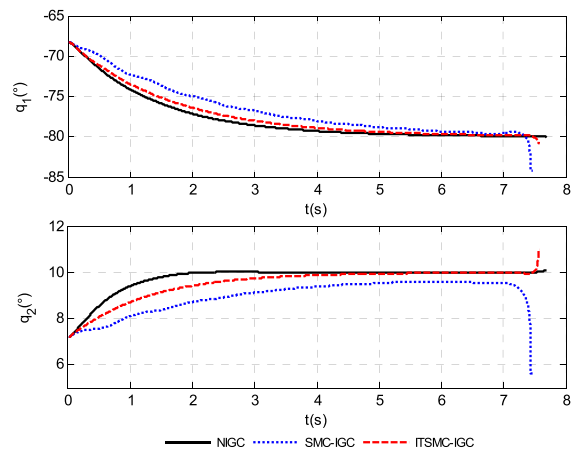


FIGURE 5. Curves of the LOS angles q_1 and q_2 in case 1.

It can be seen from both Fig. 3 and Fig. 4 that under the three IGC laws, the missiles successfully intercept the ground maneuvering targets. In Fig. 5, the LOS angles under NIGC

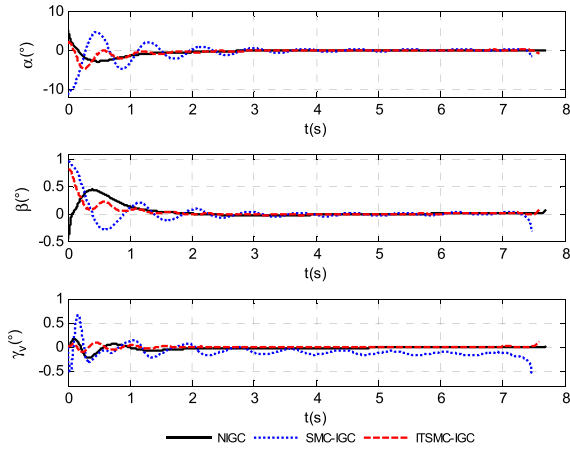


FIGURE 6. Curves of the angles α , β , and γ_v in case 1.

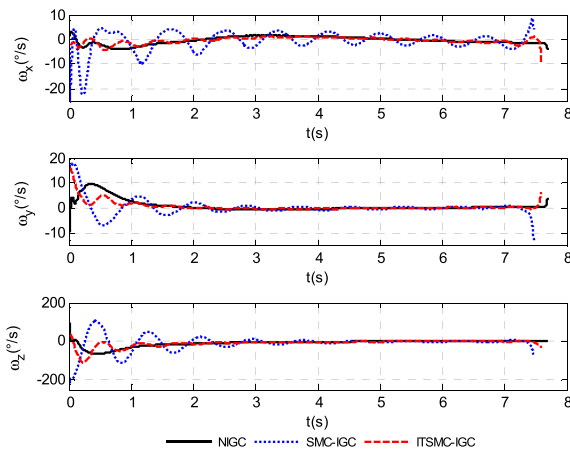


FIGURE 7. Curves of the angular rates ω_x , ω_y , and ω_z in case 1.

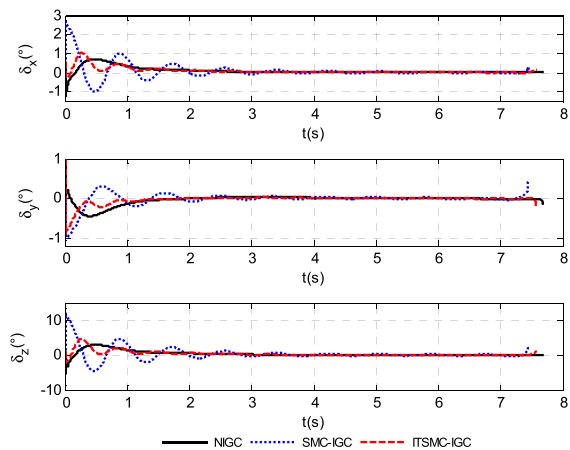


FIGURE 8. Curves of the fin deflections δ_x , δ_y , and δ_z in case 1.

law converge to the desire LOS angles in the end, whereas the missiles under SMC-IGC law and ITSMC-IGC law present large LOS angle tracking errors. And, the convergence rate for NIGC law is faster than that for SMC-IGC law and ITSMC-IGC law. Moreover, the miss distances and terminal

LOS angles under different IGC laws are list in Table 3, where q_{1t} and q_{2t} denote the terminal LOS angles. It can be found from Table 3 that the miss distance under NIGC law is smaller than that under SMC-IGC law and ITSMC-IGC law, which implies interceptive accuracy under NIGC law is better. As revealed from Fig. 6 and Fig. 7, attack angle α , sideslip angle β , velocity deflection angle γ_v , and three rotational angular velocities converge to small neighborhoods of zero under the three IGC laws. However, the convergence rate for NIGC law is faster than that for SMC-IGC law and ITSMC-IGC law. From Fig. 8, it can be observed that actuator deflections are smooth under NIGC law, however, there exist larger amplitude in the starting stage under SMC-IGC law and ITSMC-IGC law.

TABLE 3. Miss distances and terminal Los Angles of case 1.

IGC law	Miss distance (m)	q_{1t} (deg)	q_{2t} (deg)
NIGC	0.1604	-80.1245	10.0824
SMC-IGC	2.7156	-84.2908	5.644
ITSMC-IGC	0.7143	-80.7643	10.9688

Case 2: In this subsection, consider an aerial target executing sinusoidal maneuver. For the target, the velocity is set as $V_t(0) = 300$ m/s, and the flight path and heading angles at initial time are set as $\theta_t(0) = 80$ deg and $\phi_{ct}(0) = 10$ deg. The normal and tangential accelerations of the target are set as $a_n = 55 * \sin(0.5t)$ m/s² and $a_t = 55 * \sin(0.5t)$ m/s². The desired impact angles are respectively set as $q_{1f} = -80$ deg and $q_{2f} = 10$ deg. The simulation results are shown in Figs. 9-14.

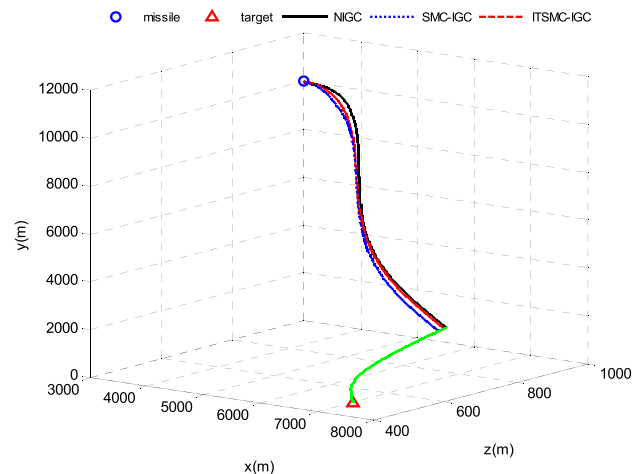


FIGURE 9. Three-dimensional trajectories of missile and target in case 2.

We can see from Fig. 9, although the trajectory may vary with each other, all three IGC laws could meet the objective of intercepting the target. As shown in Fig. 10, it can be noted that the interceptions are achieved under both laws. It is clear from Fig. 11 that the convergence rate for NIGC

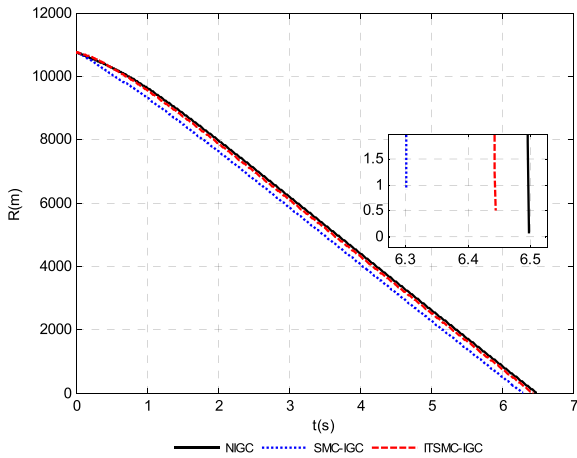


FIGURE 10. Curves of the relative distance between missile and target in case 2.

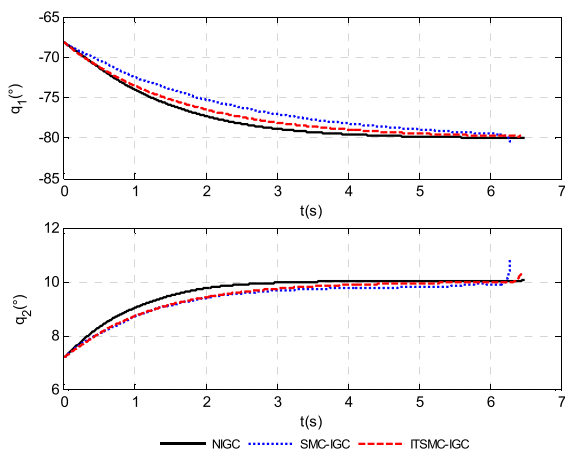


FIGURE 11. Curves of the LOS angles q_1 and q_2 in case 2.

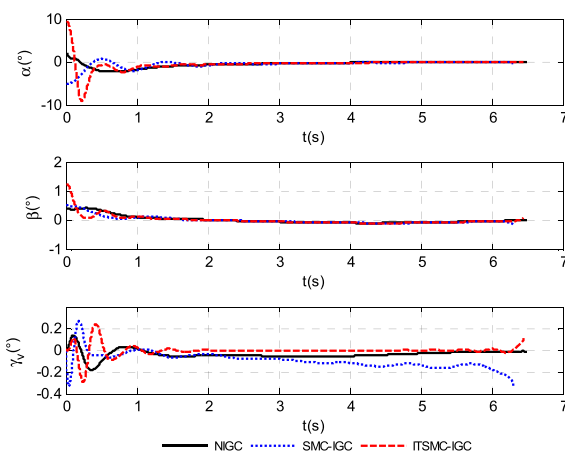


FIGURE 12. Curves of the angles α , β , and γ in case 2.

law is faster than that for SMC-IGC law and ITSMC-IGC law. The miss distances and terminal LOS angles on this occasion are listed in Table 4. The NIGC law satisfies the impact angle constraints within the impact angle errors than

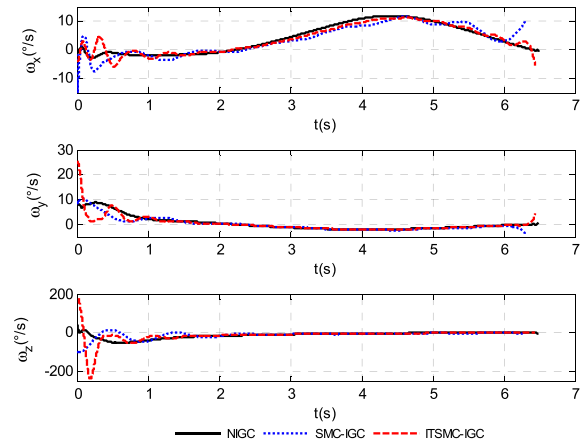


FIGURE 13. Curves of the angular rates ω_x , ω_y , and ω_z in case 2.

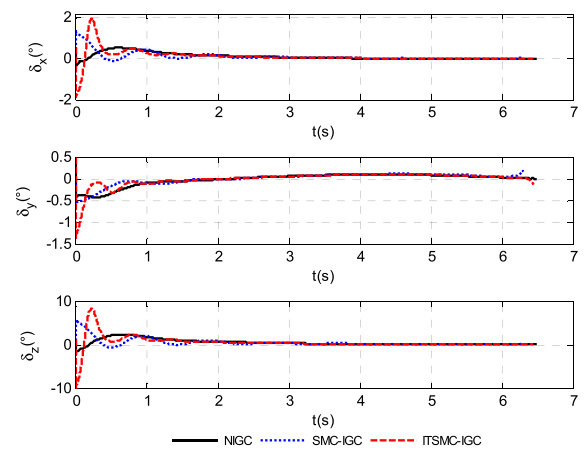


FIGURE 14. Curves of the fin deflections δ_x , δ_y , and δ_z in case 2.

TABLE 4. Miss distances and terminal Los Angles of case 2.

IGC law	Miss distance (m)	q_{1r} (deg)	q_{2r} (deg)
NIGC	0.0667	-80.0031	10.068
SMC-IGC	0.8958	-80.3286	10.8149
ITSMC-IGC	0.5197	-79.7481	10.2907

0.0031deg and 0.068deg respectively, and the miss distance less than 0.0667m. The NIGC law has smaller angle tracking errors and miss distance as compared with SMC-IGC law and ITSMC-IGC law. As revealed from Fig. 12, Fig. 13, and Fig. 14, the response curves of attack angle α , sideslip angle β , velocity deflection angle γ , rotational angular velocities, and fin deflections under NIGC law are smoother than their counterparts under SMC-IGC law and ITSMC-IGC law. Therefore, the NIGC law is more desired in terms of practical applications.

Case 3: In this subsection, similar case 1, a missile intercepts a ground maneuvering target. 200 times of Monte Carlo simulation experiments are conducted with different initial fight conditions show in Table 5 to demonstrate the robustness

TABLE 5. Monte carlo simulation parameters.

Parameter	Value	Parameter	Value
$x_m(0)$ (m)	$Unif(2940,3275)$	$\theta(0)$ (deg)	$Unif(-70,20)$
$y_m(0)$ (m)	$Unif(9665,10070)$	$\phi_c(0)$ (deg)	$Unif(-10,20)$
$z_m(0)$ (m)	$Unif(620,1230)$		

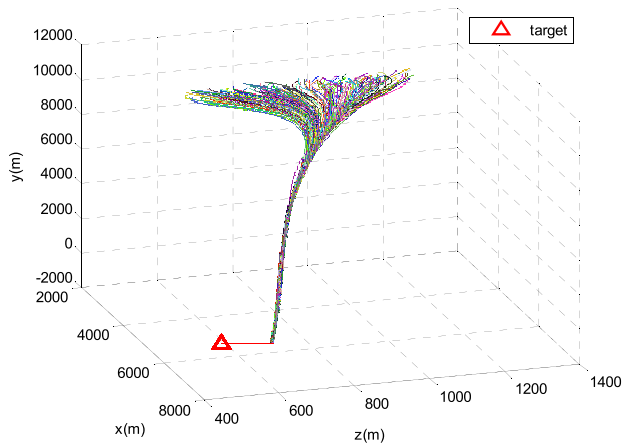


FIGURE 15. Three-dimensional trajectories of missile in Monte Carlo case.

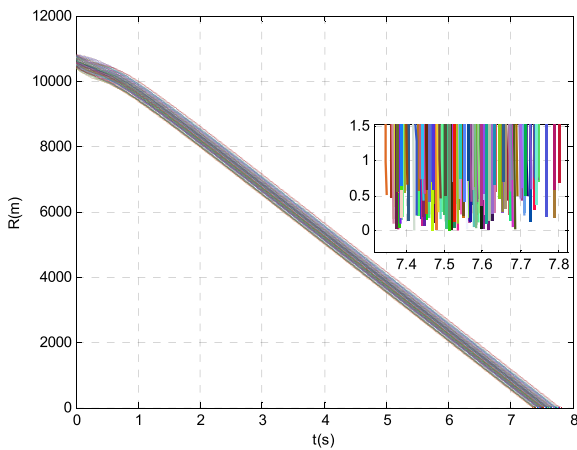


FIGURE 16. Curves of the relative distance between missile and target in Monte Carlo case.

of the proposed IGC law, where $Unif$ means a uniform distribution. The initial position, initial fight path angle, and initial heading angle of the missile are set to a uniform distribution. The desired impact angles are set as $q_{1f} = -80$ deg and $q_{2f} = 10$ deg. The trajectories, the miss distances, and the LOS angles are concerned in Figs. 15-18.

As shown in Fig. 15 and Fig.16, perfect interception of target with small miss distance is achieved in each scenario. In Fig. 17, the LOS angles converge to the desired impact angles. By means of data analysis with respect to Fig. 18, the mean and standard deviation of miss distance are found as 0.3702 meters and 0.2242 meters respectively. We can see from these figures, the proposed IGC law achieves satisfactory performance under different initial fight conditions,

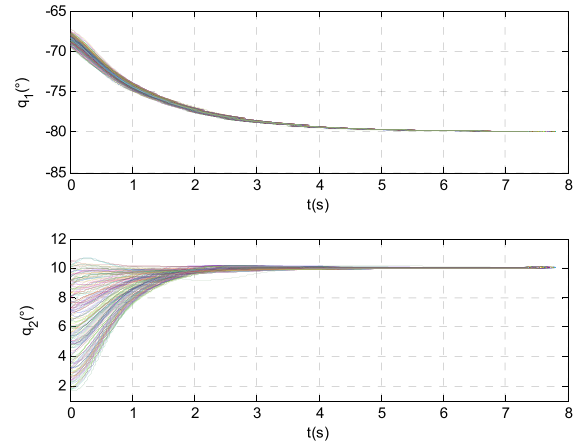


FIGURE 17. Curves of the LOS angles between missile and target in Monte Carlo case.

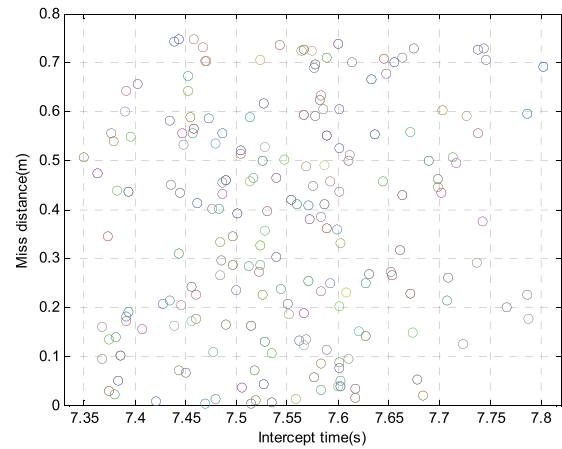


FIGURE 18. The miss distance in Monte Carlo case.

which demonstrates the robustness of the proposed IGC law. In addition, the uncertainties of the missile-related parameters have been fully considered in the Monte Carlo simulation experiments, hence it is reasonable to say that the proposed IGC law is robust with respect to the inevitable uncertainties existing in the missile dynamics.

V. CONCLUSION

In this paper, a 3-D IGC law is proposed for STT missiles considering impact angle constraint. The novel nonsingular fractional integral terminal sliding mode control scheme is presented to guarantee the system states converge to small neighborhood of zero in finite-time. The IGC law based on the novel nonsingular IFTSMC scheme is constructed for intercepting maneuvering target with the desired impact angles. Finite-time stability analysis is presented in the framework of Lyapunov function approach. The effectiveness of the proposed IGC law is demonstrated by the simulation results with some comparisons. Future work will consider the actuator failures in the proposed IGC scheme, and will put the proposed IGC scheme into practical application.

REFERENCES

- [1] D. Williams, J. Richman, and B. Friedland, "Design of an integrated strapdown guidance and control system for a tactical missile," in *Proc. Guid. Control Conf.*, 1983, pp. 57–66.
- [2] H. Yan and H. Ji, "Integrated guidance and control for dual-control missiles based on small-gain theorem," *Automatica*, vol. 48, no. 10, pp. 2686–2692, 2012.
- [3] H. Yan, S. Tan, and Y. He, "A small-gain method for integrated guidance and control in terminal phase of reentry," *Acta Astron.*, vol. 132, pp. 282–292, Mar. 2017.
- [4] X. Liu, Y. Wu, Y. Deng, and S. Xiao, "A global sliding mode controller for missile electromechanical actuator servo system," *Proc. Inst. Mech. Eng., G, J. Aerosp. Eng.*, vol. 228, no. 7, pp. 1095–1104, 2014.
- [5] J. Yun and C.-K. Ryoo, "Integrated guidance and control law with impact angle constraint," in *Proc. 11th Int. Conf. Control, Automat. Syst.*, Oct. 2011, pp. 1239–1243.
- [6] C. Bao, P. Wang, and G. Tang, "Integrated guidance and control for hypersonic morphing missile based on variable span auxiliary control," *Int. J. Aerosp. Eng.*, vol. 2019, pp. 1–20, May 2019.
- [7] S. H. Seyedipour, M. F. Jegarkandi, and S. Shamaghdari, "Nonlinear integrated guidance and control based on adaptive backstepping scheme," *Aircr. Eng. Aerosp. Technol.*, vol. 89, no. 3, pp. 415–424, 2017.
- [8] I. Eker, "Sliding mode control with PID sliding surface and experimental application to an electromechanical plant," *ISA Trans.*, vol. 45, no. 1, pp. 109–118, Jan. 2006.
- [9] S. R. Kumar, S. Rao, and D. Ghose, "Sliding-mode guidance and control for all-aspect interceptors with terminal angle constraints," *J. Guid., Control, Dyn.*, vol. 35, no. 4, pp. 1230–1246, 2012.
- [10] M. Idan, T. Shima, and O. M. Golan, "Integrated sliding mode autopilot-guidance for dual-control missiles," *J. Guid., Control, Dyn.*, vol. 30, no. 4, pp. 1081–1089, 2007.
- [11] C. Guo and X.-G. Liang, "Integrated guidance and control based on block backstepping sliding mode and dynamic control allocation," *Proc. Inst. Mech. Eng., G, J. Aerosp. Eng.*, vol. 229, no. 9, pp. 1559–1574, 2014.
- [12] T. Shima, M. Idan, and O. M. Golan, "Sliding-mode control for integrated missile autopilot guidance," *J. Guid., Control, Dyn.*, vol. 29, no. 2, pp. 250–260, 2006.
- [13] H. Mingzhe and D. Guangren, "Integrated guidance and control of homing missiles against ground fixed targets," *Chin. J. Aeronaut.*, vol. 21, no. 2, pp. 162–168, 2008.
- [14] C. Luo, J. Wang, H. Huang, and P. Wang, "Integrated guidance and control based air-to-air autonomous attack occupation of UCAV," *Math. Problems Eng.*, vol. 2016, no. 4, pp. 1–18, 2016.
- [15] C. Zhong, L. Wu, J. Guo, Y. Guo, and Z. Chen, "Robust adaptive attitude manoeuvre control with finite-time convergence for a flexible spacecraft," *Trans. Inst. Meas. Control*, vol. 40, no. 2, pp. 425–435, 2016.
- [16] L. Sun, W. Wang, R. Yi, and S. Xiong, "A novel guidance law using fast terminal sliding mode control with impact angle constraints," *ISA Trans.*, vol. 64, pp. 12–23, Sep. 2016.
- [17] A. Awad and H. Wang, "Roll-pitch-yaw autopilot design for nonlinear time-varying missile using partial state observer based global fast terminal sliding mode control," *Chin. J. Aeronaut.*, vol. 29, no. 5, pp. 1302–1312, 2016.
- [18] C. Lai, W. Wang, Z. Liu, and Z. Ma, "Three-dimensional integrated guidance and control for terminal angle constrained attack against ground maneuvering target," *Proc. Inst. Mech. Eng., G, J. Aerosp. Eng.*, vol. 233, no. 7, pp. 2393–2412, 2019.
- [19] G. Li, Z. Yu, and Z. Wang, "Three-dimensional adaptive sliding mode guidance law for missile with autopilot lag and actuator fault," *Int. J. Control, Automat. Syst.*, vol. 17, no. 6, pp. 1369–1377, 2019.
- [20] Q. Hu, T. Han, and X. Ming, "New impact time and angle guidance strategy via virtual target approach," *J. Guid. Control Dyn.*, vol. 41, no. 8, pp. 1–11, 2018.
- [21] C. Zhang and W. Yun-Jie, "Non-singular terminal dynamic surface control based integrated guidance and control design and simulation," *ISA Trans.*, vol. 63, pp. 112–120, Jul. 2016.
- [22] C. S. Chiu, "Derivative and integral terminal sliding mode control for a class of MIMO nonlinear systems," *Automatica*, vol. 48, no. 2, pp. 316–326, Feb. 2012.
- [23] L. Qiao and W. Zhang, "Adaptive non-singular integral terminal sliding mode tracking control for autonomous underwater vehicles," *IET Control Theory Appl.*, vol. 11, no. 8, pp. 1293–1306, Feb. 2017.
- [24] H. Song and T. Zhang, "Fast robust integrated guidance and control design of interceptors," *IEEE Trans. Control Syst. Technol.*, vol. 24, no. 1, pp. 349–356, Jan. 2016.
- [25] M. Hou, X. Liang, and G. Duan, "Adaptive block dynamic surface control for integrated missile guidance and autopilot," *Chin. J. Aeronaut.*, vol. 26, no. 3, pp. 741–750, 2013.
- [26] S. He, W. Wang, and J. Wang, "Three-dimensional multivariable integrated guidance and control design for maneuvering targets interception," *J. Franklin Inst.*, vol. 353, no. 16, pp. 4330–4350, 2016.
- [27] S. Xiong, W. Wang, X. Liu, Z. Chen, and Wang, "A novel extended state observer," *ISA Trans.*, vol. 58, pp. 309–317, Sep. 2015.
- [28] Z. Yao, J. Yao, and W. Sun, "Adaptive RISE control of hydraulic systems with multilayer neural-networks," *IEEE Trans. Ind. Electron.*, vol. 66, no. 11, pp. 8638–8647, Nov. 2019.
- [29] Y.-J. Si and S.-M. Song, "Continuous reaching law based three-dimensional finite-time guidance law against maneuvering targets," *Trans. Inst. Meas. Control*, vol. 41, no. 2, pp. 321–339, 2019.
- [30] L. Yan, J.-G. Zhao, H.-R. Shen, and Y. Li, "Three-dimensional united biased proportional navigation law for interception of maneuvering targets with angular constraint," *Proc. Inst. Mech. Eng., G, J. Aerosp. Eng.*, vol. 229, no. 6, pp. 1013–1024, 2015.
- [31] W. Wang, S. Xiong, S. Song, and C. Lai, "Three dimensional impact angle constrained integrated guidance and control for missiles with input saturation and actuator failure," *Aerosp. Sci. Technol.*, vol. 53, pp. 169–187, Jun. 2016.
- [32] S. Yang, J. Guo, and J. Zhou, "New integrated guidance and control of homing missiles with an impact angle against a ground target," *Int. J. Aerosp. Eng.*, vol. 2018, pp. 1–10, Aug. 2018.
- [33] J. H. Wang, "Active disturbance rejection guidance and control scheme for homing missiles with impact angle constraints," *Proc. Inst. Mech. Eng., G, J. Aerosp. Eng.*, vol. 233, no. 3, pp. 1133–1146, 2019.
- [34] X. Liu, W. Huang, and L. Du, "An integrated guidance and control approach in three-dimensional space for hypersonic missile constrained by impact angles," *ISA Trans.*, vol. 66, pp. 164–175, Jan. 2017.
- [35] S.-H. Song and I.-J. Ha, "A Lyapunov-like approach to performance analysis of 3-dimensional pure PNG laws," *IEEE Trans. Aerosp. Electron. Syst.*, vol. 30, no. 1, pp. 238–248, Jan. 1994.
- [36] S. Yu, X. Yu, R. Stonier, B. Shirinzadeh, and Z. Man, "Continuous finite-time control for robotic manipulators with terminal sliding mode," *Automatica*, vol. 41, no. 11, pp. 1957–1964, 2005.
- [37] S. Peng and W. Shi, "Adaptive fuzzy integral terminal sliding mode control of a nonholonomic wheeled mobile robot," *Math. Problems Eng.*, vol. 2017, pp. 1–12, Apr. 2017.



XINGHE ZHOU was born in Henan, China, in 1993. He received the M.S. degree from Harbin Engineering University, Harbin, China, in 2017. He is currently pursuing the Ph.D. degree in navigation, guidance and control with Beihang University, Beijing, China. His research interests include nonlinear control, guidance, and integrated guidance and control.



WEIHONG WANG received the B.S., M.S., and Ph.D. degrees from the Harbin Institute of Technology, Harbin, China, in 1990, 1993, and 1996, respectively. She is currently a Professor of automation science and electrical engineering, and a Ph.D. Tutor with Beihang University, Beijing, China. Her research interests include computer simulation, computer control and simulation, guidance, intelligent control, servo control, and simulation technique.



ZHENGHUA LIU received the B.E. and M.S. degrees from the Nanjing University of Aeronautics and Astronautics, Nanjing, China, in 1997 and 2000, respectively, and the Ph.D. degree from Beihang University, Beijing, China, in 2004, where he is currently an Associate Professor with the School of Automation Science and Electrical Engineering. His research interests include high precision servo control, robotic systems, and flight control.



CHAO LAI received the B.E. degree from Dalian Maritime University, Dalian, China, in 2013, and the Ph.D. degree from Beihang University, Beijing, China, in 2019. He is currently with Navigation and Control Technology Research Institute of China North Industries Group Corporation. His research interests include nonlinear control, servo control, adaptive control, and integrated guidance and control.

...



CHEN LIANG received the B.E. degree from the Harbin Institute of Technology, Weihai, China, in 2012, and the M.S. degree in electrical and computer engineering from Rutgers, The State University of New Jersey, New Brunswick, NJ, USA, in 2014. He is currently pursuing the Ph.D. degree in navigation, guidance and control with Beihang University, Beijing, China. His research interests include nonlinear control, machine vision, and deep learning and guidance.